Flammability properties of polymer nanocomposites with single-walled carbon nanotubes: effects of nanotube dispersion and concentration[☆]

Takashi Kashiwagi[a,*], Fangming Du[b], Karen I. Winey[c], Katrina M. Groth[a], John R. Shields[a], Severine P. Bellayer[a], Hansoo Kim[c], Jack F. Douglas[d]

[a]*NIST, Building and Fire Research Laboratory, Fire Research Division, Gaithersburg, MD 20899, USA*
[b]*University of Pennsylvania, Chemical and Biomolecular Engineering Department, Philadelphia, PA 10194, USA*
[c]*University of Pennsylvania, Materials Science and Engineering Department, Philadelphia, PA 10194, USA*
[d]*NIST, Materials Science and Engineering Laboratory, Polymers Division, Gaithersburg, MD 20899, USA*

Abstract

The effects of the dispersion and concentration of single walled carbon nanotube (SWNT) on the flammability of polymer/SWNT nanocomposites were investigated. The polymer matrix was poly (methyl methacrylate) (PMMA) and the SWNT were dispersed using a phase separation ('coagulation') method. Dispersion of SWNTs in these nanocomposites was characterized by optical microscopy on a micrometer scale. Flammability properties were measured with a cone calorimeter in air and a gasification device in a nitrogen atmosphere. In the case where the nanotubes were relatively well-dispersed, a nanotube containing network structured layer was formed without any major cracks or openings during the burning tests and covered the entire sample surface of the nanocomposite. However, nanocomposites having a poor nanotube dispersion or a low concentration of the nanotubes (0.2% by mass or less) formed numerous black discrete islands with vigorous bubbling occurring between these islands. Importantly, the peak heat release rate of the nanocomposite that formed the network layer is about a half of those, which formed the discrete islands. It is proposed that the formation of the discrete islands is due to localized accumulation of the nanotubes as a result of fluid convection accompanying bubble formation and rise of the bubbles to the surface through the molten sample layer and bursting of the bubbles at the surface. The network layer acts as a heat shield to slow the thermal degradation of PMMA.
© 2004 Elsevier Ltd. All rights reserved.

Keywords: Nanocomposite; Single walled carbon nanotube; Flammability

1. Introduction

There is a high level of interest in using filler particles having at least one nano-dimensional scale (nanofiller) for making polymeric nanocomposite materials with exceptional properties [1,2]. One of the promising applications involves the improvement in flammability properties of polymers with nanofillers because one weak aspect of polymers is that they are combustible under certain

conditions. These filled systems are attractive as possible alternatives to conventional flame retardants and furthermore they could simultaneously improve both physical and flammability properties of polymers. At present, the most common approach using nano scale particles is the use of layered silicates having large aspect ratios. The flame retardant (FR) effectiveness of clay-polymer nanocomposites with various resins has been demonstrated and several flame retardant mechanisms have been proposed [2–10]. It appears that the flammability properties of clay-polymer nanocomposites are not significantly affected by whether they are intercalated or exfoliated as long as they are nanocomposites rather than microcomposites. Significant reduction in heat release rate has been achieved with a clay content of about 5% by mass.

Carbon nanotubes are another candidate as a FR additive because of their highly elongated shape (high aspect ratio). This was demonstrated by using multi-walled carbon nanotubes (MWNT) in polypropylene (PP) [11,12] and also in poly(ethylene vinyl acetate) [13]. The in situ formation of a continuous, network structured protective layer from the tubes is critical for significant reduction in heat release rate, because the layer thus acts as a thermal shield from energy feedback from the flame [12]. Single-walled nanotubes also have potential as flame retardants by the same mechanism. Despite reports of the exceptional physical properties of the nanocomposites with SWNT [14–17], there are no published studies on the flammability of SWNT polymer nanocomposites. The dispersion of SWNT in polymers remains a challenge, so it is important to determine the effects of the nanotube dispersion on flammability properties. Thus, we investigate the effects of small quantities of single-walled carbon nanotubes and their dispersion in PMMA on the flammability properties of these nanocomposites.

2. Experimental

2.1. Materials

The matrix polymer used in this paper is poly(methyl methacrylate) (PMMA) (Polysciences,[1] M_w: 100,000 g/mol). SWNTs for the nanocomposites were synthesized by the high-pressure carbon monoxide method (HiPCo)[18]. The metal residue in the SWNTs is less than 13% by mass. The coagulation method was used to produce the SWNT/PMMA nanocomposites [17]. In the coagulation method, dimethylformamide (DMF) was chosen to dissolve the PMMA and to permit dispersion of the SWNT by bath sonication for 24 h. To obtain good nanotube dispersion, the nanotube concentration in DMF is critical. Our atomic force microscopy (AFM) results show that the average nanotube bundle diameter increases with an increase of the nanotube concentration in DMF, from ∼7 nm at the concentration of 0.2 mg (SWNT) per ml (DMF) to ∼13 nm at 0.4 mg/ml. We can observe nanotube agglomerates at a concentration higher than 0.4 mg/ml by the naked eye, while the 0.2 mg/ml suspension is visually homogeneous. Therefore, we can control the nanotube dispersion in the nanocomposites by changing the nanotube concentration in DMF, assuming that the state of nanotube dispersion is comparable in DMF before coagulation and in the polymer matrix after coagulation suspension [19]. Concentrations of 0.2 and 1 mg/ml were used to make nanocomposites with good and poor dispersion, respectively. The content of the nanotubes

in the nanocomposites varied from 0.2% to 1% by mass. The notation of the PMMA/SWNT(0.5%) means that the sample contains 0.5% by mass of SWNT in PMMA.

All samples were compression molded at 210 °C under a pressure of 6 metric tons to make 75 mm diameter by 4 mm thick disks for the measurement of heat release rate and 8 mm thick disks for the gasification measurement in a nitrogen atmosphere.

2.2. Sample characterization

The morphologies of the nanotubes in PMMA were examined in transmission by optical microscopy. A hot press was used to prepare nanocomposite films of ∼30 μm in thickness, which were examined by an optical microscope (Olympus, BH-2) with a magnification of 200 to study the global dispersion of SWNTs. The morphology of the nanocomposites residues after the nitrogen gasification tests was investigated using scanning electron microscopy (SEM) (JEOL 6300FV, at 5 kV). The transmission electron microscopy (TEM), JEOL 2010 operated at 200 kV, was used for original SWNT and collected residues after the gasification tests. The collected residue was gently crushed with a mortar and dispersed in ethanol with a 15 min sonication. The bright field (BF) TEM images were recorded with a charge-coupled device (CCD) with the resolution of 1024×1024 pixels.

Thermal gravimetric analyses (TGA) were conducted using a TA Instruments TGA Q 500 at 5 °C/min from 90 to 500 °C in nitrogen (flow rate of 60 cm³/min) for the original nanocomposite samples (∼8 mg) in a platinum pan and from 90 to 900 °C in nitrogen for the SWNTs and for the residues collected after nitrogen gasification tests. The standard uncertainty in sample mass measurement is ±1%. The complex viscosity of the sample was measured using a Paar Physica UDS 200 Rheometer. The sample was located between a stationary and an oscillating plate at 0.1 rad/s (low shear simulating burning condition of the sample) from 190 to 280 °C at an a heating rate of 1 °C/min in nitrogen.

2.3. Flammability property measurement

A cone calorimeter built by NIST was used to measure ignition characteristics, heat release rate, and sample mass loss rate according to ASME E1354/ISO 5660. An external radiant heat flux of 50 kW/m² was applied. All of the samples were measured in the horizontal position and wrapped with thin aluminum foil except for the irradiated sample surface. The standard uncertainty of the measured heat release rate was ±10%.

A radiant gasification apparatus, somewhat similar to a cone calorimeter, was designed and constructed at NIST to study the gasification processes of samples by measuring mass loss rate and temperatures of the sample exposed to a fire-like heat flux in a nitrogen atmosphere (no burning). The apparatus consists of a stainless-steel cylindrical

chamber that is 1.70 m tall and 0.61 m in diameter. In order to maintain a negligible background heat flux, the interior walls of the chamber are painted black and the chamber walls are water-cooled to 25 °C. All experiments were conducted at 50 kW/m². The unique nature of this device is threefold: (1) observation and results obtained from it are only based on the condensed phase processes due to the absence of any gas phase oxidation reactions and processes; (2) it enables visual observations of gasification behavior of a sample using a video camera under a radiant flux similar to that of a fire without any interference from a flame; (3) the external flux to the sample surface is well-defined and nearly constant over the duration of an entire experiment (and over the spatial extent of the sample surface) due to the absence of heat feedback from a flame. A more detailed discussion of the apparatus is given in our previous study [20]; the standard uncertainty of the measured mass loss rate is ±10%.

3. Results

3.1. Sample morphology

The distribution of the nanotubes in PMMA/SWNT(0.5%) was examined by optical microscopy to globally observe the dispersion of the nanotubes, as shown in Fig. 1. Fig. 1(a) indicates that the nanotubes are relatively uniformly distributed within the polymer matrix on a micrometer scale. By using a higher concentration of SWNT in the DMF suspension, the sample in Fig. 1(b) shows regions of nanotube aggregation. In this study, the former sample is designated as having 'good dispersion' and the latter sample is designated as having 'poor dispersion'. The TEM image of the purified original SWNT shows many nanotube bundles with a small amount of amorphous carbon and of large carbon fullerenes with many iron particles in the nanotubes from the residual catalyst, as shown in Fig. 1(c). The SEM image shown in the previous study indicates that approximately 20 nm diameter nanotubes bundles such as shown in Fig. 1(c) are uniformly distributed on a sub-micrometer scale [17].

3.2. Thermal stability

Thermal gravimetric analysis was conducted in nitrogen. Although previous studies did not conclusively exclude the effects of oxygen in surrounding air on thermal degradation of polymeric materials during burning of the polymers, oxidation reactions of the polymers appear to be insignificant (oxygen is mainly consumed by gas phase reactions i.e., the flame). Exception is the case in which the flame does not cover the entire burning surface or the burning/pyrolysis rate is extremely low [21,22]. Either addition of SWNTs to PMMA or the distribution of nanotubes in PMMA does not show significant effects on the thermal stability of PMMA,

as shown in Fig. 2. On the other hand, results previously published for the acrylonitrile–butadiene–styrene (ABS)/SWNT samples showed that the addition of SWNT reduced the thermal stability of ABS at higher mass fractions of nanotubes than those used in this study [23].

3.3. Complex melt viscosity

During a nitrogen gasification tests, both liquid-like behavior and solid-like behavior of the nanocomposite samples were observed as described later in this paper. Thus, complex viscosities of the PMMA/SWNT samples were measured as a function of temperature (at a heating rate of 1 °C/min in nitrogen) at a constant frequency rate of 0.1 rad/s which was selected as representing the low shear rates during burning. The results are shown in Fig. 3. Complex viscosity significantly increases with an increase of SWNT content especially at higher temperatures. With 1% by mass of SWNT, complex viscosity of the nanocomposite increases at least one order above that of pure PMMA. The slope of the relationship between complex viscosity and temperature tends to gradually decrease with an increase of SWNT content in the nanocomposite. Furthermore, at the composition of 0.5% by mass the nanocomposite with poor nanotube dispersion exhibits much lower complex viscosity than that with good nanotube dispersion at high temperatures.

3.4. Effects of dispersion of SWNT on flammability properties

Heat release rate histories of the three different samples, PMMA, PMMA/SWNT(0.5%) and PMMA/SWNT(0.5%, poor dispersion), were measured at an external radiant flux of 50 kW/m²; the results are shown in Fig. 4. The heat release rate of the sample with good nanotube dispersion of the nanotubes is much lower than those of pure PMMA and of the sample with poor dispersion. The heat release rate of the sample with poor dispersion is not appreciably reduced from that of PMMA. However, the total heat releases of all samples (integrated value of heat release rate with respect to time) are comparable. This indicates that the sample with relatively good nanotube dispersion burns much slower than that with poor nanotube dispersion but both samples eventually burn almost completely.

It is important to understand how the difference in dispersion of the nanotubes affects heat release rate of the nanocomposite. In order to answer this question, the behavior of the two samples during the gasification test in a nitrogen atmosphere was observed by taking video movies. Selected pictures from the video images are shown in Fig. 5. For the sample with good nanotube dispersion, numerous small bubbles formed initially and their bursting was observed at the surface. This was shortly followed by a solid-like behavior with no overt fluid motion. A slightly wavy solid surface and gradual receding of the
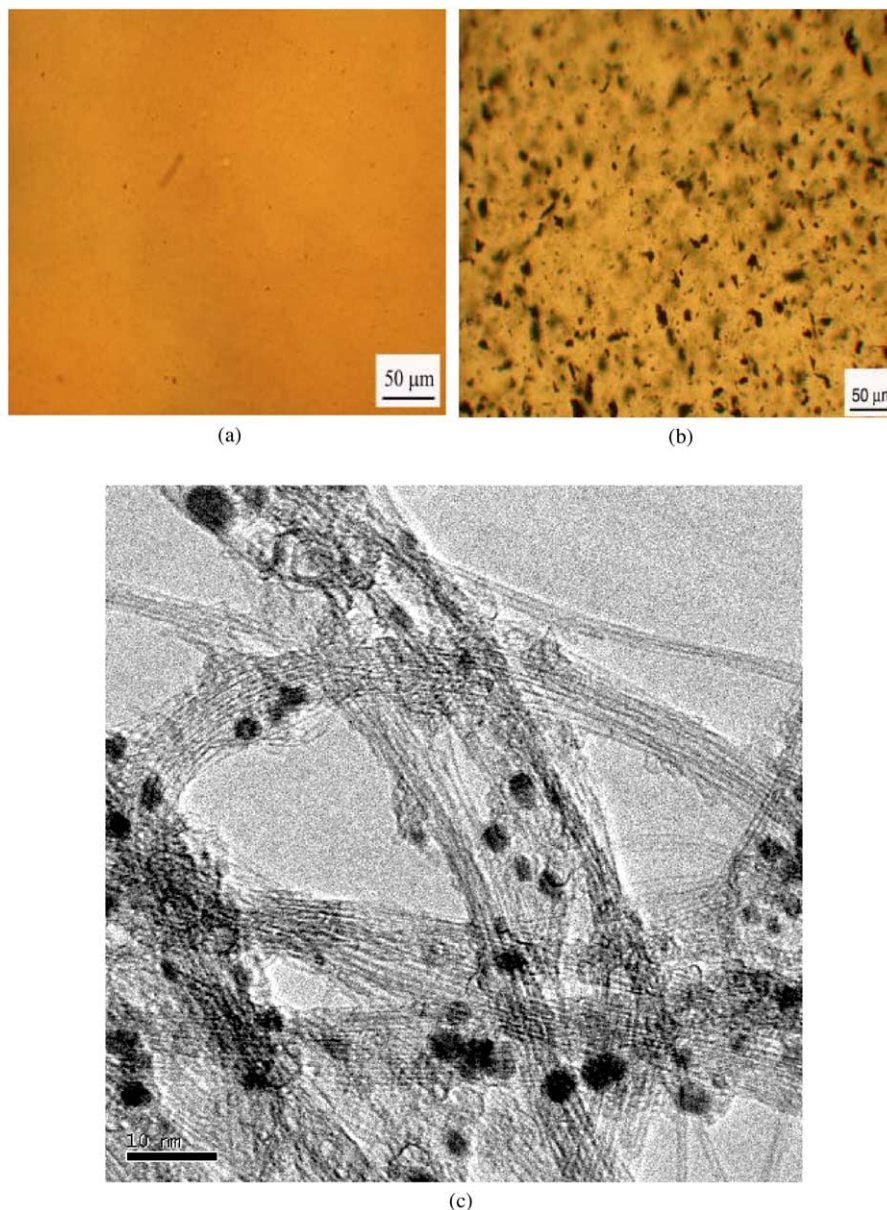
Fig. 1. Optical micrographs of PMMA/SWNT(0.5%) with two different dispersion of nanotubes, (a) 'good dispersion' and (b) 'poor dispersion' with numerous agglomerates. (c) TEM image of original SWNT.

sample surface were observed over the test period. The sample with poor nanotube dispersion formed initially many small bubbles and their bursting at the surface was followed by the formation of many small black discrete islands. Vigorous bubbling was subsequently observed between the islands. At a later time, the islands coalesced into a connected structure and their size gradually increased during the course of the test. The mass loss rate curves of samples with good and poor nanotube dispersion are plotted in Fig. 6 along with that of pure PMMA for comparison. The results clearly show that the dispersion of the nanotubes is critical for reduction in mass loss rate. This trend is the same as that observed for the heat release rate curves, as shown in Fig. 4. This confirms that the effects of the dispersion of the

nanotubes on flammability properties are based on a physical or chemical process in the condensed phase.

The residues of PMMA/SWNT(0.5%) were collected after the completion of the gasification tests (8 mm thick sample) and also of cone calorimeter (burning) tests (4 mm thick sample). The pictures of the residues are shown in Fig. 7. Both residues of the samples with good dispersion of nanotubes were covered by a continuous dark layer compared to many black islands for the residues of the samples with poor nanotube dispersion. Glowing combustion of the residues shortly after the burning tests was observed. The pictures of the burned residues show faint orange color and a small amount of ash. Similar observation was made for the PP/MWNT nanocomposites and glowing
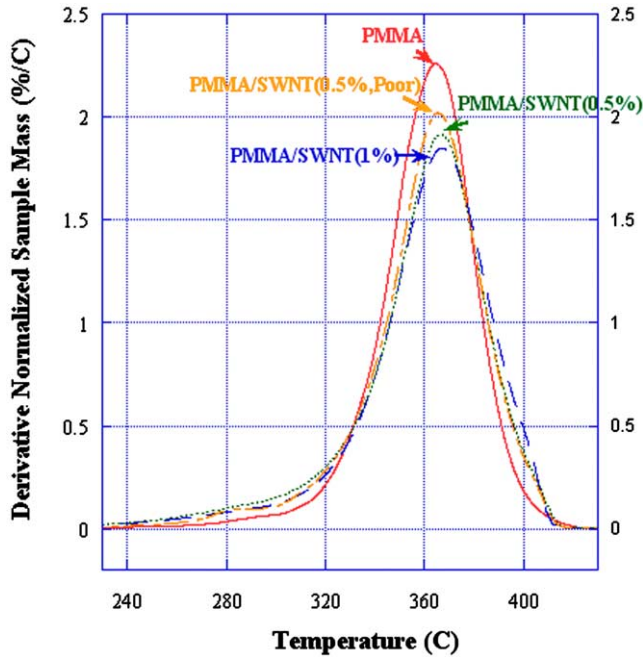
Fig. 2. Derivative thermogravimetric mass loss rates of selected samples at heating rate of 5 °C/min in nitrogen.

combustion was due to oxidation of MWNTs with surrounding oxygen in air (no more flaming at the end of the test), which was enhanced by iron from the residual catalyst for synthesizing the nanotubes [12]. The orange color of the burned residues was caused by the formation of iron oxide. It is assumed that observed glowing combustion in this study is also due to the oxidation enhanced by the residual iron in the original SWNT as seen in Fig. 1(c). Smaller islands in the burned residue (Fig. 7(d)) that those in
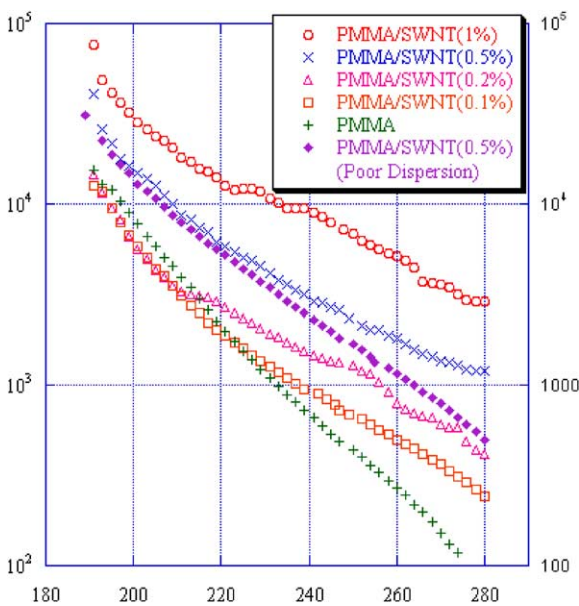
Fig. 3. Effects of the addition of SWNT on complex viscosity of PMMA at 0.1 rad/s in nitrogen.
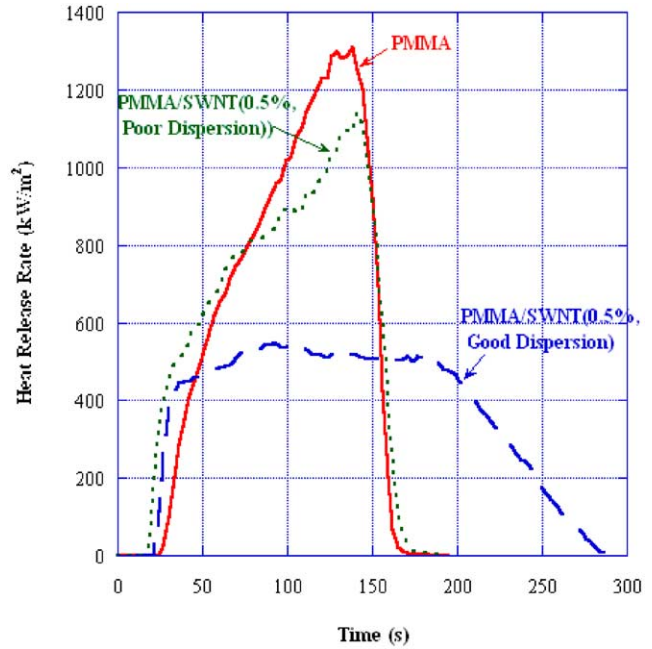

Fig. 4. Effect of SWNT dispersion on heat release rate of PMMA/SWNT(0.5%) nanocomposite at external radiant flux of 50 kW/m^2.

the gasified residue in nitrogen (Fig. 7(c)) were due to glowing combustion at the end of the burn test, which consumed some of the residue during cooling after removing the residue from the cone calorimeter.

3.5. Effects of SWNT concentration on flammability properties

Heat release rate curves of various PMMA/SWNT nanocomposites having good dispersion of the nanotubes were measured; the results are shown in Fig. 8. The addition of 0.1% by mass of SWNT did not significantly reduce the
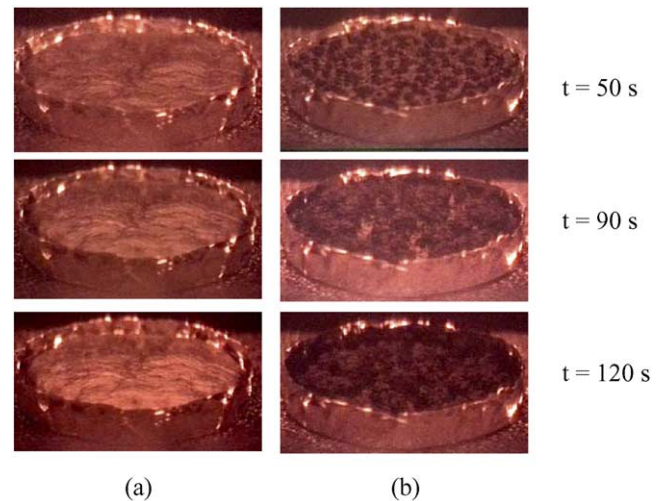

Fig. 5. Selected video images of PMMA/SWNT(0.5%) during gasification tests at 50 kW/m^2 in nitrogen; (a) with good nanotube dispersion and (b) with poor nanotube dispersion.
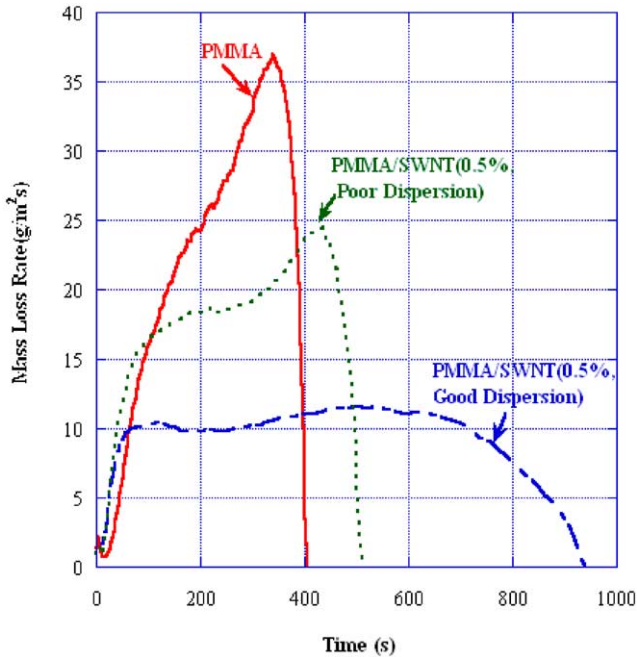
Fig. 6. Effect of SWNT dispersion on mass loss rate of PMMA/SWNT at 50 kW/m^2 in a nitrogen atmosphere.

Fig. 8. Effects of SWNT concentration on heat release rate curve of PMMW/SWNT at 50 kW/m^2.

heat release rate of PMMA. A roughly 25% reduction in the peak heat release rate was achieved by the addition of 0.2% by mass of the nanotubes. The most reduction in heat release rate was achieved by 0.5% by mass. All nanocomposite samples ignited earlier than pure PMMA and this trend is due to the increase in surface absorptivity of the nanocomposites compared to lower surface absorptivity of PMMA (by absorption bands) with respect to broad emission spectra (grey body) of the cone calorimeter heater [12].

The sample behavior was observed during the gasification test in a nitrogen atmosphere to understand the effects of the concentration of the nanotubes on mass loss rate curve. As expected, the PMMA sample melted and behaved like a liquid accompanied by numerous bubbles and their bursting at the sample surface, as shown in Fig. 9(a). At the end of the test, no residue was left behind as shown in Fig.
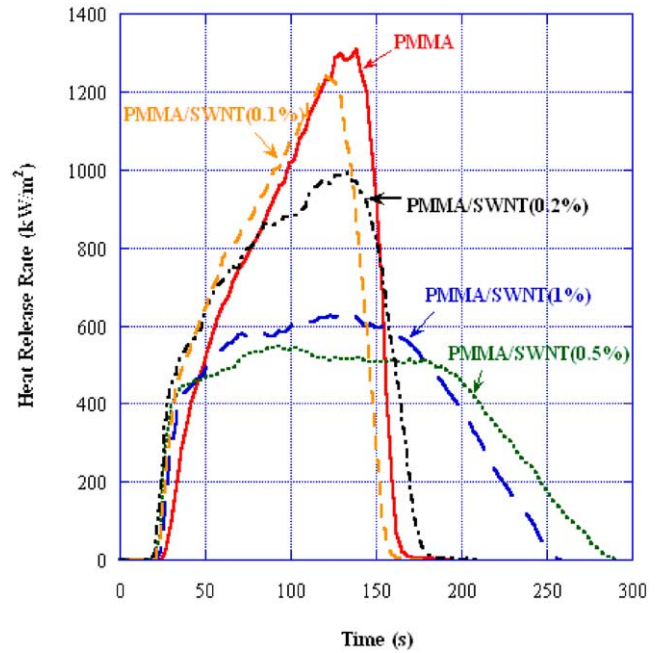
10(a). For the nanocomposite sample with 0.2% mass fraction of the nanotubes, many small, black discrete islands were formed after initial numerous small bubbles and their bursting at the surface. Bubbling was observed between islands and it appeared that bubbling pushed nanotubes to the islands and the size of islands gradually became larger and eventually some of the islands were connected to each other. The connected black islands were left behind at the end of the test, as shown in Fig. 10(b). This picture is very similar to the one for PMMA/SWNT(0.5%, poor dispersion), as shown in Fig. 7(c). For the samples with 0.5% by mass and 1% by mass, both samples appeared to be solid-like; a network layer covered the sample surface during the entire test period and was left behind without any major cracks at the end of the test, as shown in Figs. 10(c) and (d).

The measured mass loss rate curves of all samples tested in a nitrogen atmosphere are shown in Fig. 11. The trend of
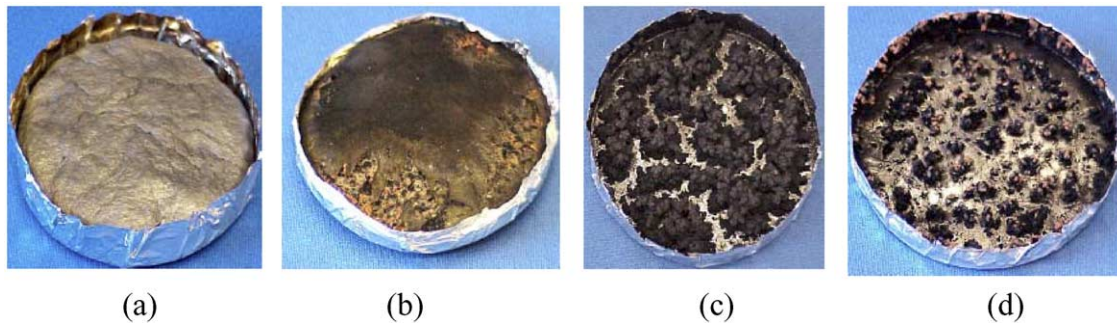

Fig. 7. Effects of dispersion of nanotubes on pictures of residues of PMMA/SWNT(0.5%) (note 8 mm thick sample for the gasification test and 4 mm thick for the burning test); (a) nitrogen gasification residue, good dispersion sample (b) burned residue, good dispersion sample (c) nitrogen gasification residue, poor dispersion sample (d) burned residue, poor dispersion sample.
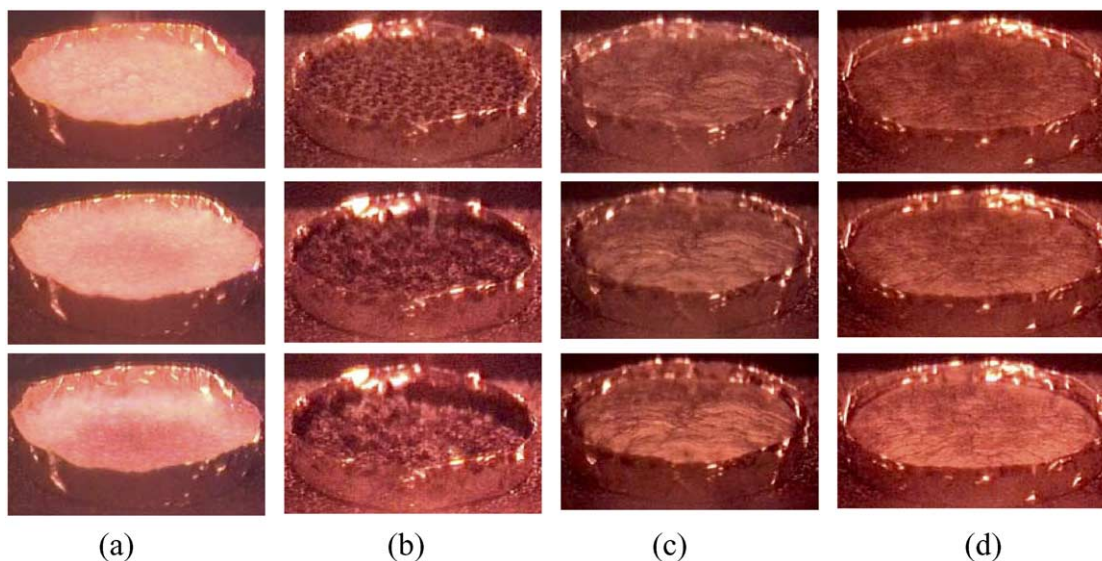
Fig. 9. Selected video images of PMMA/SWNT during gasification tests at external radiant flux of 50 kW/m² in a nitrogen atmosphere, (a) PMMA, (b) PMMA/SWNT(0.2%), PMMA/SWNT(0.5%), and (d) PMMA/SWNT(1%).

the curves is similar to that of the heat release rate curves shown in Fig. 8. This clearly indicates that the observed effects of the concentration of SWNT on the flammability properties are based on physical processes in the condensed phase (thermal stability results of the nanocomposites show little effect due to the concentration of the tubes, as shown in Fig. 2).

4. Discussion

The formation of a protective network layer covering the entire surface without any cracks or openings is critical for reducing the heat release rate and mass loss rate of the nanocomposites. Therefore, it is important to understand how the black discrete islands are formed instead of the formation of the continuous layer and how to avoid them. In the early stage of the gasification test, the upper part of the sample is heated and starts melting. When the temperature of the sample becomes high enough, degradation starts to generate methyl methacrylate (MMA) as the main degradation product [24]. Because the degradation temperature of

PMMA (shown in Fig. 2) is much higher than the boiling temperature of MMA (100 °C), MMA is superheated and nucleates, forming bubbles in the melt layer. With the addition of the nanotubes, it is quite possible that heterogeneous nucleation initiated by numerous nanotubes accelerates the formation of bubbles. The bubbles rapidly rise (and expand) to the sample surface if the surrounding layer is a melt with low viscosity. The melt viscosities of the sample containing SWNT at 0.1% by mass and 0.2% by mass are low (particularly at high temperatures). Therefore, the gasification of both PMMA/SWNT(0.1%) and PMMA/SWNT(0.2%) samples behaved like a liquid, with vigorous bubbling. Then, the bubbles induce convective movement through the molten layer as they rise to the surface where they burst. This disrupts any accumulating layer consisting of the nanotubes (even a nanotube network is formed in the initial sample). As bubbles rise and burst at the surface, the nanotubes are pushed away from bubble areas and accumulate to form small discrete islands. This proposed mechanism of the formation of many small islands is illustrated in Fig. 12(a). Because the regions between the islands were exposed to an undiminished external radiant
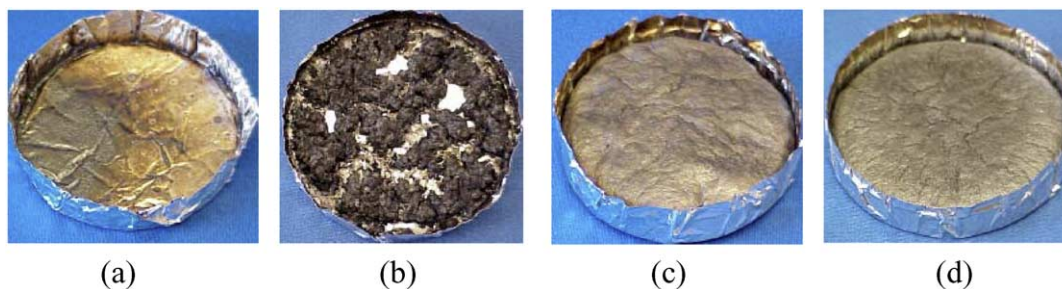

Fig. 10. Pictures of the residues of PMMA/SWNT after the gasification tests in a nitrogen atmosphere at external radiant flux of 50 kW/m². (a) PMMA, (b) PMMA/SWNT(0.2%), (c) PMMA/SWNT(0.5%), (d) PMMA/SWNT(1%).
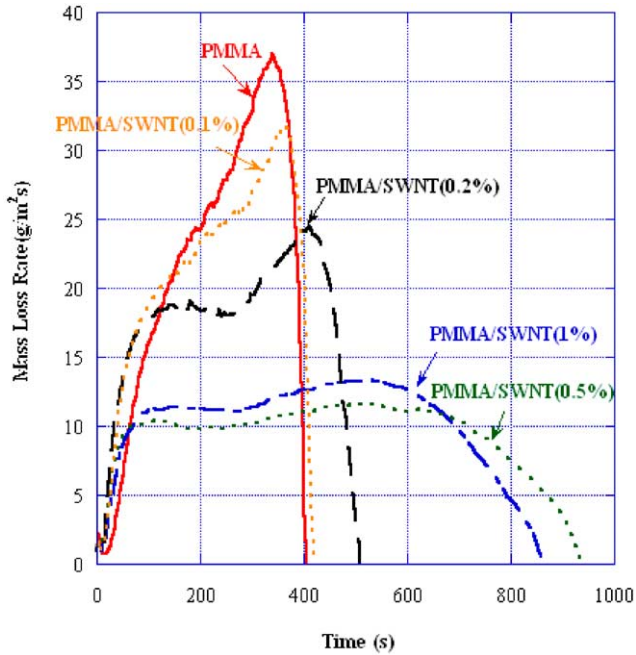
Fig. 11. Effects of SWNT concentration on mass loss rate of PMMA/SWNT at external radiant flux of 50 kW/m^2 in a nitrogen atmosphere.

flux, vigorous bubbling and bursting occurred preferentially between the islands. This is the reason why the mass loss rate and heat release rate of the samples with 0.1% and 0.2% by mass of SWNT are much higher than those of samples containing higher content of nanotubes. A similar process also occurred with the PMMA/SWNT(0.5%, poor dispersion) sample due to low melt viscosity (in particular at high temperatures) even with the same amount of the nanotubes in the sample.

The melt viscosities of the samples with 0.5% and 1%

mass fractions of the nanotubes are high enough to behave like a solid material during the gasification test. The bubbles remain small in the high viscosity layer and their transport to the surface tends not to disrupt the structured layer, such that the layer is preserved during gasification and burning. (Other possibilities are; (1) bubble size is related to viscosity and low viscosity allows for bubble coalescence while high viscosity does not, (2) the nanocomposites tend to generate smaller bubbles by nucleation from well-dispersed, high content of the nanotubes and the nanotube network inhibits the formation of large bubbles.) This proposed mechanism for the formation of the network structured layer is described for the sample containing higher contents of the nanotubes in Fig. 12(b). To form this structured layer, both a sufficient amount of nanotubes and their good, micrometer scale dispersion in a polymer are required in order to form such layer.

The importance of the formation of the protective layer on the reduction in heat release rate of the nanocomposite has been clearly demonstrated. However, the characterization of the protective layer is needed to understand how it reduces heat release rate. The SEM image of the residue of PMMA/SWNT(1%) shows a network structure consisting of bundled, inter-wined carbon nanotubes, as shown in Fig. 13. The residue was strong enough to be readily handled without breaking it. However, the sample studied in this work shrank during the gasification test and the thickness of the residue was about 3 mm for PMMA/SWNT(0.5%) and about 3.5 mm for PMMA/SWNT(1%). This thickness is much less than the, approximately, 7 mm thickness of the residue of PP/MWNT(1%). Possible reasons for this difference could be that the aspect ratio of the MWNT (large diameter, long tubes) was larger than that of the SWNT (very small, relatively short tubes) or the size
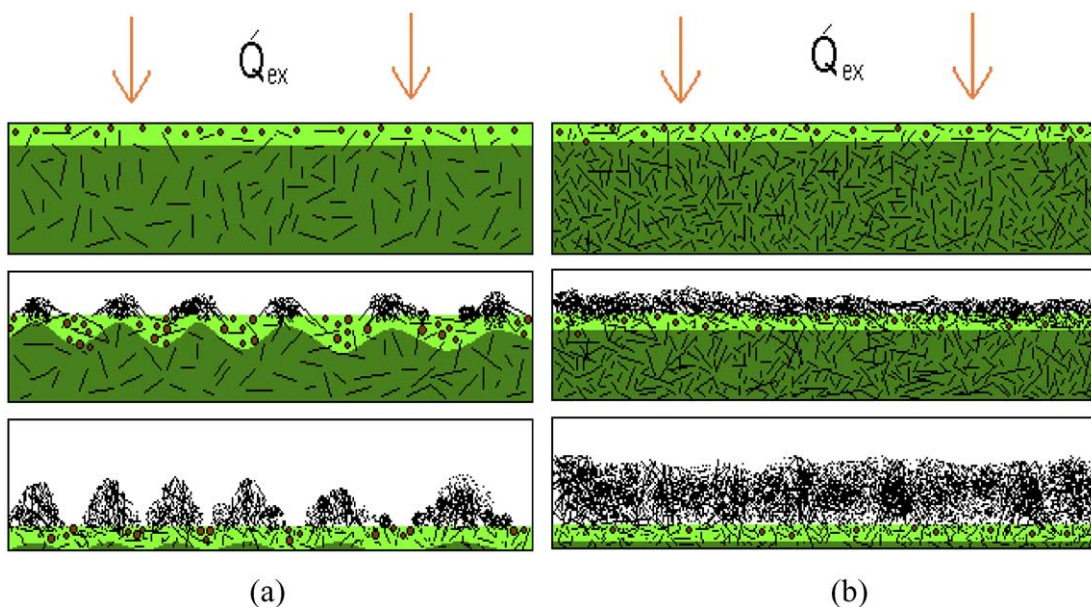

Fig. 12. Schematic illustration of the formation of islands (a) and of a network structured layer (b). Light color represents a melt layer. Circles are bubbles.
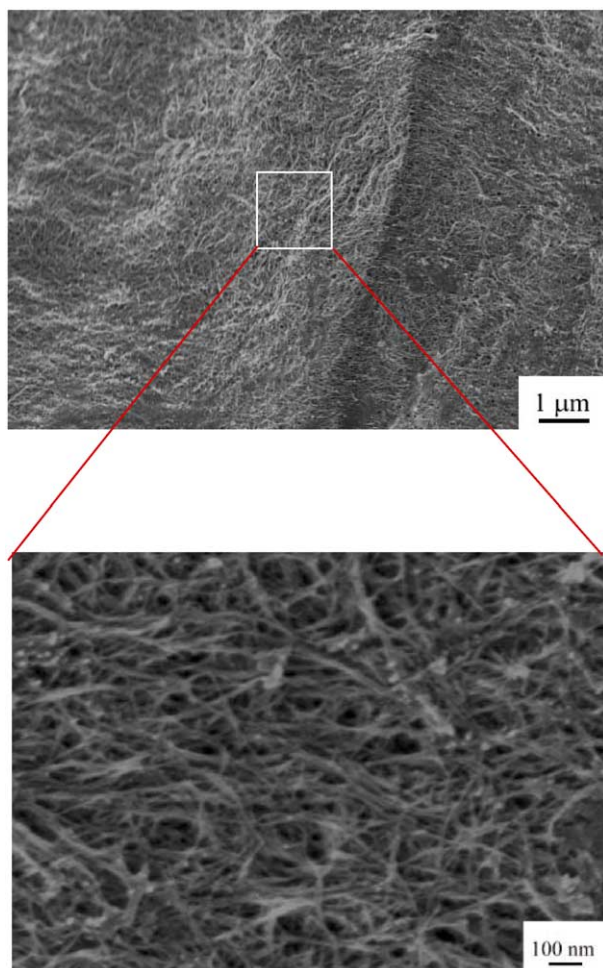
Fig. 13. SEM image of the residue of PMMA/SWNT(1%) collected after nitrogen gasification indicating a randomly interlaced structure.

distribution of the former was very large compared to relatively narrow size distribution of the latter. The network structured layer consisted of the large size distribution and high aspect ratios of the tubes might yield a physically stronger layer than that consisted of the nanotubes having the narrow size distribution and small aspect ratios.

The amount of each residue collected after the gasification test was measured and is listed in Table 1. The results indicate that the addition of the nanotubes slightly increases the amount of the residue from PMMA. The sample with poor nanotube dispersion generates less residue compared to that with good nanotube dispersion. This could be due to more confinement of PMMA and MMA by the network layer than by the discrete islands. Thermal analysis of the

residue was conducted to determine the thermal stability of the top layer of the residue and the results were compared with that of the bottom layer of the residue (the top layer appeared to be a continuous, pasty looking material compared to a more porous, granular structure for the bottom layer). Furthermore, the results might indicate any hydrocarbons in the residue assuming that the nanotubes themselves are thermally stable (no mass loss) in the temperature range used in the TGA in nitrogen. The TGA results of the original PMMA/SWNT(0.5%), original SWNT, and the top layer and bottom layer of the residue of PMMA/SWNT(0.5%) collected after the nitrogen gasification test are shown in Fig. 14. Each test was conducted using ultra high purity nitrogen at a heating rate of 5 °C/min from 90 to 900 °C after holding 90 min at 90 °C for removing any moisture trapped in the sample (Note that nitrogen purity was critical, because oxygen impurities were found to approximately double the mass loss in the SWNT and residues). Surprisingly, about 21% mass of the original SWNT was lost by 900 °C. This could be caused by thermal degradation of amorphous carbon and large carbon full-erenes as impurities as observed in Fig. 1(c). The top layer lost about 13% mass of the original residue and the bottom layer lost about 20% mass of the original residue. The residue tends to be more thermally stable than the original SWNT. This is due to 'cleaning' of the nanotubes in the sample by heating during the gasification test. It is estimated that the temperature of the top layer during the gasification experiment reached at most 650 °C (assuming that the radiant source temperature of the top layer emits a radiant flux equal to the flux difference from the incident flux minus the transmitted flux of about 12 kW/m^2 through the residue layer as described later). By 650 °C, this figure shows about 9% mass loss of the original SWNT. It appears that SWNT in the top layer of the residue lost about 9% of the original SWNT mass during the gasification test (The heating duration in the gasification test was at most 15 min. The TGA results shown in Fig. 14 indicates little mass loss of SWNT from 650 to 725 °C (temperature increase during 15 min at 5 °C/min heating rate).). Then, the nanotubes in the top layer of the residue contain about 12% of thermally degradable impurities by 900 °C. The mass loss from the top residue is about 13% by 900 °C. Therefore, the top residue consists of about 99% of its mass of the nanotubes with about 1% by mass of newly formed residue. This indicates that the top layer of the residue consists almost entirely of the nanotubes. The estimated temperature of the bottom layer is a little over 400 °C (assuming that the radiant source

Table 1

Mass fractions of the residues normalized by the original sample mass collected after the gasification test

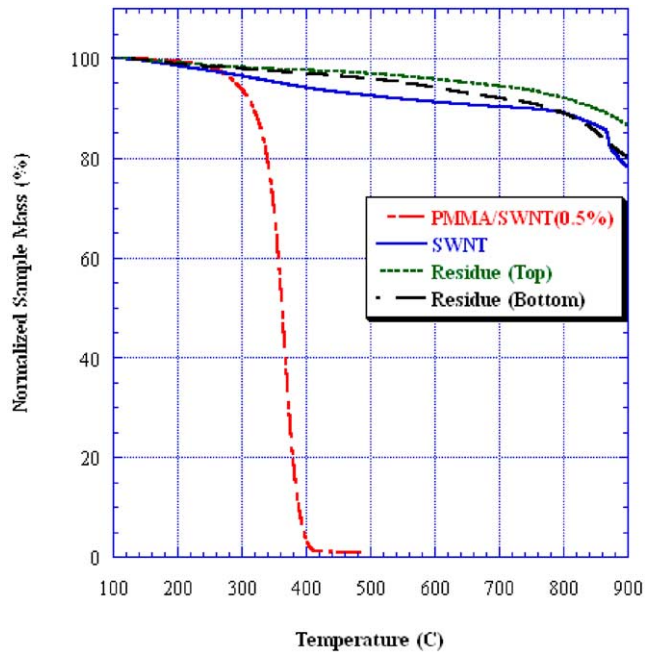| Mass fraction of SWNT(%)	0.0	0.2	0.5[a]	0.5	1.0
Residue mass/original mass (%)	0.0	0.068 ± 0.05	0.76 ± 0.05	0.99 ± 0.05	1.81 ± 0.05

[a] Poor dispersion.

Fig. 14. TGA results of PMMA/SWNT(0.5%), SWNT, and the residue of PMMA/SWNT(0.5%) collected after the gasification test, top is top layer and bottom is bottom layer of the residue, at 5 C/min in nitrogen.

Fig. 15. TEM image of the bottom layer of the residue of PMMA/SWNT(0.5%) collected after the gasification test.

temperature emits $12 \, kW/m^2$ of the flux) which is high enough to degrade PMMA. In this temperature range, the nanotubes loose about 5% by mass. The bottom layer of the residue looses about 20% of by mass by 900 °C and it consists of about 4% by mass of newly formed residue (20% -(21%–5%)) and about 96% by mass of the nanotubes. TEM images of the bottom layer of the residue show bundles of the nanotubes coated with amorphous carbon and residual iron particles (Fig. 15).

The thermal characteristics of the network structured layer are important in determining the flame retardant effectiveness of the PMMA/SWNT nanocomposites. A test was conducted to measure the transmission of a broadband external radiant flux and also the thermal insulation performance of this layer. The test was conducted in the gasification device in a nitrogen atmosphere to avoid any exothermic glowing combustion of the layer in air. At first, the external radiant heat source was turned on with the closed water cooled shutter over the residue until the heat source reached a steady temperature emitting a steady flux of about $51 \, kW/m^2$. Then, the shutter was opened by a pneumatic piston and the residual layer was exposed to the external radiant flux. The layer was directly mounted on (and in contact with) a water cooled Gardon type flux gauge (diameter of 15 mm) which recorded heat flux through the layer. The recorded transmitted flux of about $12 \, kW/m^2$ through the residual layer of the PMMA/SWNT(0.5%) sample is shown in Fig. 16. The flux gage sees a combination of transmitted external radiant flux plus a part of re-emission from the hot layers. The results show that the gauge detected the steady-state value of transmitted
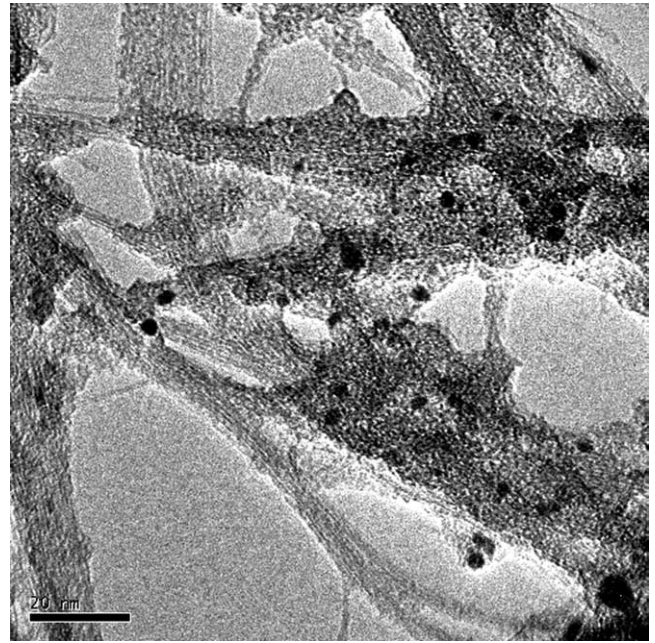
flux almost instantly within 2–3 s from the start of opening of the shutter, (full opening took about 1 s, the response of the gauge was about 1 s, and data were taken every 1 s). Another important aspect of the results is that the transmitted flux remained constant during a 6 min period. This means that thermal conduction through the network
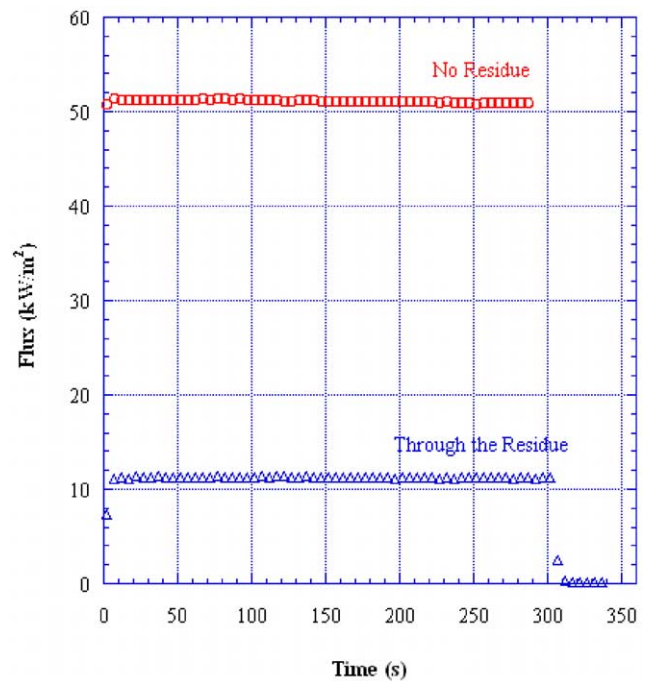

Fig. 16. Transmission characteristics of the residue of PMMA/SWNT(0.5%) collected from the gasification test at $51 \, kW/m^2$ in nitrogen. A shutter was closed shortly after 300 s with the residue.

layer appears to be negligible compared to radiative transfer. The external radiant flux of 51 kW/m^2 was absorbed at the top layer of the residue and heated the layer nearly instantaneously due to its low density (about 0.03 g/cm^3 for the residue of PMMA/SWNT(0.5%)). The hot top layer re-emitted radiation to the gas phase as a heat loss and also to the inside of the residue. Since the heat-up time of the layer was almost instantaneous due to its low density, achievement of steady-state radiative transfer through the residue was very quick. The network structured layer acts as a thermal shield to reduce the exposure of the polymer resin in the nanocomposite to an external radiant flux or to heat feedback from a flame.

5. Conclusion

PMMA/SWNT nanotube nanocomposites were prepared by the coagulation method and the effects of nanotube dispersion and concentration (up to 1% by mass) on the flammability properties of these nanocomposite were determined. A nanotube-containing network structured layer without any major cracks or openings was formed during the burning tests and covered the entire sample surface of the nanocomposite having good nanotube dispersion. However, the nanocomposite having poor nanotube dispersion or a low content of the nanotubes (0.2% by mass or less) formed numerous black discrete islands and vigorous bubbling was observed between the islands. The peak heat release rate of the nanocomposite which formed the network structured layer is about a half less than those which formed the islands. It is proposed that the formation of the islands is due to localized accumulation of the nanotubes as a result of bubble bursting at he surface and bubble-induced flow from inside the sample to the surface through the molten sample layer. Bubbles are formed from nucleation of the degradation product (methyl methacrylate) of PMMA. The network structured layer consists of mainly the nanotubes with a small amount of hydrocarbons and amorphous carbon. The layer acts as a heat shield to slow the thermal degradation of PMMA.

Acknowledgements

References

[1] Giannelis E. Adv Mater 1996;8(1):29–35.
[2] Gilman JW, Kashiwagi T. SAMPE J 1997;33(44):40–6.
[3] Zhu J, Morgan AB, Lamelas J, Wilkie CA. Chem Mater 2001;13: 3774–80.
[4] Zanetti M, Camino G, Mulhaupt R. Polym Degrad Stab 2001;74: 413–7.
[5] Gilman JW, Jackson CL, Morgan AB, Harris Jr RH, Manias E, Giannelis EP, Wuthernow M, Hilton D, Phillips SH. Chem Mater 2000;12:1866–73.
[6] Zhu J, Uhl FM, Morgan AB, Wilkie CA. Chem Mater 2001;13: 4649–54.
[7] Alexandre M, Beyer G, Henrist C, Cloots R, Rulmont A, Jerome R, Dubois P. Macromol Rapid Commun 2001;22:943–6.
[8] Zhu J, Start P, Mauritz A, Wilkie CA. Polym Degrad Stab 2002;77: 253–8.
[9] Morgan AB, Harris RH, Kashiwagi Jr T, Chyall LJ, Gilman JW. Fire Mater 2002;26:247–53.
[10] Kashiwagi T, Harris Jr RH, Zhang X, Briber RM, Cipriano BH, Raghavan SR, Awad WH, Shields JR. Polymer 2004;45:881–91.
[11] Kashiwagi T, Grulke E, Hilding J, Harris R, Awad W, Douglas J. Macromol Rapid Commun 2002;23:761–5.
[12] Kashiwagi T, Grulke E, Hilding J, Groth K, Harris R, Butler K, Shields J, Kharchenko S, Douglas J. Polymer 2004;45:4227–39.
[13] Beyer G. Fire Mater 2002;26:291–3.
[14] Haggermueller R, Gommans HH, Rinzler AG, Fischer JE, Winey KI. Chem Phys Lett 2000;330:219.
[15] Ajayan PM, Schadler LS, Giannaris C, Rubio A. Adv Mater 2000;12: 750–3.
[16] Mamedov AA, Kotov NA, Prato M, Guldi DM, Wicksted JP, Hirsch A. Nature Mater 2002;1:190–4.
[17] Du F, Fischer JE, Winey KI. J Polym Sci: Part B, Polym Phys 2003; 41:3333–8.
[18] Nikolaev P, Bronikowski MJ, Bradley RK, Rohmund FR, Colbert DT, Smith KA, Smalley RE. Chem Phys Lett 1999;313:91.
[19] Du F, Scogna RC, Zhou W, Brand S, Fischer JE, Winey KI. Macromolecules 2004 [in press].
[20] Austin PJ, Buch RR, Kashiwagi T. Fire Mater 1998;22:221–37.
[21] Brauman SK. J Polym Sci Chem Ed 1975;26:1159–71.
[22] Kashiwagi T, Ohlemiller TJ. Proc Combust Inst 1982;19:815–23.
[23] Yang S, Castilleja JR, Barrera EV, Lozano K. Polym Degrad Stabil 2004;83:383–8.
[24] Madorsky SL. Thermal degradation of organic polymers. New York: Interscience; 1964 [Chapter 8].